Journal of the Korean Ceramic Society
Vol. 48, No. 6, pp. 577~583, 2011.

http://dx.doi.org/10.4191/kcers.2011.48.6.577

Electron Spin Resonance (ESR) and Microwave Absorption Studies of Superparamagnetic Iron Oxide Nanoparticles (SPIONs) for Hyperthermia Applications

Yongho Choi, Terry Yi*, Joo Seok Park*, and Do Kyung Kim**,†**

Department of Materials Science and Engineering, Jungwon University, Goesan 367-805, Korea
**Department of Sports Medicine, Jungwon University, Goesan 367-805, Korea*
***Department of Biomedical Science, Jungwon University, Goesan 367-805, Korea*
****Korea Institute of Ceramic Engineering and Technology, Seoul 153-801, Korea*

(Received September 26, 2011; Revised October 23, 2011; Accepted October 25, 2011)

ABSTRACT

Stabilized biocompatible superparamagnetic iron oxide nanoparticles (SPIONs) were prepared by controlled coprecipitation method for hyperthermia application. ESR measurements determined that all of the interactions in the individual SPIONs (1 nm and 11 nm) were antiferromagnetic in nature because the ions contributed to the magnetization with a range of magnetic moments. In-situ monitoring of the temperature increment was performed, showing that the microwave absorption rate of the SPIONs was dispersed in an appropriate host media (polar or non-polar solvents) during microwave irradiation. Microwave absorption energy rates and heat loss of SPIONs in solvent were calculated by non-linear data fitting with an energy balance equation. The microwave absorption rates of SPIONs dispersed in solvent linearly increases when the concentration of SPIONs increases, implying that the microwave absorption rate can be tunable by changing the concentration of SPIONs.

Key words : Magnetite, Superparamagnetic, Iron oxide, Nanoparticles, Microwave absorption, ESR, SPIONs

1. Introduction

Current available treatments for cancer patients include hyperthermia,[1] chemotherapy,[2] radiation therapy,[3] surgery, gene therapy,[4] and immunotherapy.[5] Hyperthermia is the generation of heat; with respect to cancer therapy, hyperthermia is treatment wherein heat is generated at the tumor site, changing the physiology of diseased cells and finally leading to apoptosis. Methods for heating the whole body include using hot wax, hot air, hot water suits, infrared, radiofrequency (RF), microwave, ultrasound, hot blood, and blood perfusion. Experimental and clinical reports indicate that local heating has promising potential for hyperthermia therapy, but it is difficult to generate and regulate the temperature in tumors and normal tissues while minimizing the deleterious effects of hyperthermia. One way to control the temperature is by manipulating two important magnetic properties of the magnetic nanoparticles: magnetization and coercivity. These two properties are related to the heating efficiency and Curie temperature, so they can be adjusted slightly above the therapeutic temperature. Self-regulating heating mediators could potentially be developed once methods for sufficient heating are improved.[6]

†Corresponding author : Do Kyung Kim
E-mail : dokyung@jwu.ac.kr
Tel : +82-43-830-8606 Fax : +82-43-830-8679

In thermal ablation, a tumor is subjected to high temperatures (> 46°C, up to 56°C) causing cells to undergo direct tissue necrosis, coagulation or carbonization. Moderate hyperthermia (41°C < T < 46°C) has various effects at both the cellular and tissue levels. Diathermia uses lower temperatures (T < 41°C) to treat rheumatic diseases in physiotherapy. During moderate hyperthermia, which is traditionally termed as hyperthermia treatment, cells undergo heat stress in the temperature range of 41-46°C, resulting in activation and/or initiation of many intra- and extracellular degradation mechanisms, such as protein denaturation, protein folding, aggregation, and DNA cross-linking. With a single heat treatment, permanent irreversible protein damage can occur, resulting in protein aggregation and/or inhibition of many cellular functions.[7]

Several reasons have been suggested for the limited amount of heat arising in tumor tissue during hyperthermia treatment. The temperature difference between the tumor and surrounding normal tissue are generally attributed to the difference in blood flow in normal tissue. Another possible reason is that tumor cells are sensitive to heat due to their hypoxic, acidic, and poor nutritional states. During hyperthermia treatment, the heating also increases the membrane permeability of some drugs, which has led to hyperthermia being combined with chemotherapy.

In magnetic fluid hyperthermia (MFH),[8] superparamagnetic iron oxide nanoparticles (SPIONs) are intravenously injected into the body as mediators that selectively diffuse into cancerous tissues. When a high-frequency alternating magnetic field

(AMF) is added, the SPIONs heat up, raising the temperature of the tumor cells without adverse effects to the surrounding healthy tissue. The generated heat can be controlled using SPIONs with an adaptable Curie temperature, which is tunable by varying the chemical compositions, particle size, and surface modifications of the SPIONs.

SPIONs have recently been highlighted in various nano-medicinal areas, as MR imaging agents, drug delivery vectors, drug-targeting agents, and as hyperthermia mediators via intravenous or extravenous injection. For example, in the early stages of tumors, it is difficult to diagnose and identify lesions using only MR imaging, because of its low sensitivity and limited detection. The intensity of the MRI signal must be drastically enhanced through the introduction of contrast agents, i.e. paramagnetic Gd-EDTA and SPIONs, which induce precession and resonance more than water molecules. Furthermore, SPIONs techniques can also be used for in vitro gene transfection. In this case, a high-field, high-gradient is positioned under the multi-well plate, culture flask, or petri dish in which the cells are growing. The fundamental principle is that therapeutic agents are attached to, or encapsulated within, micro- or nanoparticles. These carrier vectors may have magnetic cores with biocompatible and biodegradable polymers, which can be further functionalized with therapeutic chemicals, or they may consist of mesoporous polymers that contain SPIONs precipitated inside the pores. By functionalizing the polymer or metal coating, it is possible to attach (for example) cytotoxic drugs for targeted chemotherapy or therapeutic DNA to correct a genetic defect.[9)]

When an electromagnetic field is used as energy deposition, the influencing aspects are a complex function of frequency, intensity, polarization of the applied fields, geometry, and size of the SPIONs. Several variable factors need to be taken into account to regulate the desired target temperature for hyperthermia, including electron spin resonance (ESR),[10)] energy deposition, thermal conductivity in the membrane, and particle transports between the membranes. Extensive technical effort, advanced therapy, and thermometric systems are required to resolve these issues, because experimental hyperthermia requires thermal homogeneity in target legions with a controlled temperature.

Whether or not the SPIONs are administrated to the tissue, ESR is the major phenomenon under external magnetic field, RF, or microwave irradiation. Microwave heating devices for hyperthermia are already commercially available, using frequencies of 434 MHz, 915 MHz and 2,450 MHz. These devices use a microwave generator, including a helical antenna, which is moderately different from the conventional microwave oven, used as a household appliance. The specially designated microwave heating device for hyperthermia can localize the frequency on the target area, i.e. the lesion, instead of full body heating. In general, an output frequency of 915 MHz with a maximum power of 60 watts is permitted for medical use, because it requires no RF shield enclosure. It is well known that water molecules can be stimulated by a 2,450 MHz microwave, which is used for household appliance. Because of this, that frequency range is not optimistic for medical uses, because organs and cells include an abundance of water molecules. Even though 2,450 MHz microwave is not a proper frequency for hyperthermia, this frequency can be used to interpret the microwave absorption and heating mechanisms of SPIONs, because the absorption mechanisms will be similar to other microwave frequency ranges. However, a non-polar solvent was used, since polar solvents can be stimulate by a 2,450 MHz microwave. For the case of polar solvent, the heating profile of the solvent was recorded as a control experiment and subtracted from the heating profiles of SPIONs dispersed in solvent.

To predict the proper amount of SPIONs and the appropriate exposure time to SPIONs for in-vivo hyperthermia, this study analyzes the heating mechanisms of SPIONs in non-polar solvent under microwave irradiation. We suggest and demonstrate indirect interpretation of the microwave absorption rate by monitoring the temperature increment of SPIONs dispersed in either polar or non-polar solvents during microwave irradiation. In the same manner, this approach will be useful for predicting the amount of SPIONs and the exposure time when microwave generators of any frequency range are used as heating devices. For example, SPIONs dispersed in oil can be can be used as a column heater, and the heating element can be replaced by a magnetron. In this case, heating and energy efficiency will be much higher than a conventional oil heater, similar to the case of a microwave oven. To design such an appliance, the amount of SPIONs and exposure time must be calculated based on the suggested approach.

2. Experimental Procedure

2.1. Materials

All chemicals were of reagent grade and were used without further purification. Ferric chloride hexahydrate ($FeCl_3 \cdot 6H_2O$ > 99%), ferrous chloride tetrahydrate ($FeCl_2 \cdot 4H_2O$ > 99%), sodium hydroxide (NaOH, 99%), and concentrated hydrochloride (HCl, 99%, 12N) were obtained from Sigma-Aldrich. Milli-Q water was re-deionized (specific conductance < 0.1 s/cm) and deoxygenated by flowing N_2 gas for 1 h prior to use.

2.2. Preparation of superparamagnetic iron oxide nanoparticles (SPIONs)

SPIONs with an average particle size of 1 nm were prepared without any additional stabilizer according to the following procedure. Typically, 5 mL of iron solution containing 1×10^{-2} M Fe^{2+} and 2×10^{-2} M Fe^{3+} was added dropwise into 50 mL of 8×10^{-1} M NaOH under vigorous mechanical stirring (2,000 min^{-1}) for 30 min at room temperature. The color of the suspension changed to black almost immediately. SPIONs with a particle size of 11 nm were prepared by increasing the reaction temperature. All of the procedures and experimental conditions were the same as the above procedure, except 1×10^{-1} M Fe^{2+} and 2×10^{-1} M Fe^{3+} was added dropwise into 50 mL of 8×10^{-1} M NaOH alkaline solution. The product was heated to 80°C for 30 min under magnetic stirring. The precipitated powders were collected and removed from the solution by

applying an external magnetic field. The supernatant solution was removed from the precipitate after decantation. Deoxygenated Milli-Q water was added to wash the powder and the solution was decanted after centrifugation at 3,500 min^{-1}. After washing the powder three times, 1×10^{-2} M HCl solution was added to neutralize the anionic charge on the surface of the particles. The positively charged colloidal particles were then separated by centrifugation and peptized by adding deoxygenated Milli-Q water. For ESR measurements, the sample was dried in a vacuum oven at 120°C for 12 h. Based on the XRD measurements, the size of SPIONs nanoparticles was 1 and 11 nm.

2.3. Microwave absorption

A commercially available microwave oven operating at a maximum power level of 800 W was used in this study. The oven was equipped with a K-type thermocouple attached to a data acquisition system using a PC. The diameter of the thermocouple is important for increasing S/N inside the microwave cavity. A stainless steel shield with a diameter of 1.5 mm was used to effectively shield the thermocouple from the microwave field. Domestic microwave ovens operate over the entire power range in alternating cycles, from maximum to zero.[11] The frequency of the maximum power cycle is represented by a power level number. For example, power level 2 means that the magnetron is actually on for an average of 2 s out of every 10 s, whereas power level 10 represents continuous radiation.

100 mL of cyclohexane/toluene containing a certain amount of magnetite was placed in a Teflon container and inserted into the microwave cavity. All the experiments were performed at a fixed volume (100 mL) and a fixed container position in the cavity. Microwave enhancements were determined by comparing the data sets obtained using similar time steps of microwave irradiation.

2.4. Characterization of SPIONs

A TEM study was carried out on a JEOL-2000EX microscope with an electron kinetic energy of 200 kV. The specimen for TEM imaging was prepared by suspending the SPIONs in deionized water by sonication for 3 min. After ultrasonic dispersing, 1 mL of the SPIONs suspension was centrifuged for 5 min at 14,000 min^{-1}. A drop of well-dispersed supernatant was placed on a carbon-coated 200 mesh copper grid, and the sample was then dried under ambient conditions before being attached to the sample holder on the microscope.

The Electron Spin Resonance (ESR) measurements were performed as a function of temperature with average particle sizes of 1 and 11 nm in diameter. The ESR spectra were recorded with a Bruker spectrometer operating in the X band (9.5 GHz) and interfaced to a PC with Stelar software for data acquisition and handling. The sample was mounted in a microwave cavity placed between two poles of an electromagnet, providing a DC field up to 1.6 T. An Oxford continuous helium gas flow cryostat, operating in the temperature ranges 4-300 K, was used to study the temperature dependence of the different sized SPIONs. A commercial temperature controller was used to adjust the temperature, having an accuracy of 1 K. The relative orientation of the external field and the experimental sample axes was determined with a goniometer. The magnetic field component of the microwave field always remained perpendicular to the DC field. Small amplitude, 100 kHz AC magnetic field was applied parallel to the DC field in order to record the field-derivative ESR absorption signal.

3. Results and Discussion

3.1. Synthesis and characterization of magnetite nanoparticles

The chemical reaction of Fe_3O_4 precipitation is given by:

$$Fe^{2+} + 2\ Fe^{3+} + 8\ OH^- \rightarrow Fe_3O_4 + 4\ H_2O \quad (1)$$

According to the results of thermodynamic modeling of this system, a complete precipitation of Fe_3O_4 is expected in the pH range pH = 7.5-14, while maintaining a molar ratio of Fe^{2+} : Fe^{3+} = 1 : 2 under a non-oxidizing environment. Under oxidizing conditions, Fe_3O_4 may be oxidized, as given by the following equations:

$$Fe_3O_4 + 0.25\ O_2 + 4.5\ H_2O \rightarrow 3Fe(OH)_3 \quad (2)$$

$$Fe_3O_4 + 0.25O_2 + \rightarrow 1.5Fe_2O_3 \quad (3)$$

Aqueous dispersion of superparamagnetic iron oxide nanoparticles was prepared by adding an aqueous mixture of ferric and ferrous salts to a strong alkaline solution at room temperature. In the present study, a solution of NaOH was used as alkali source, instead of ammonia. Oxygen is eliminated from the solution by flowing N_2 gas through the reaction medium during synthesis operation in a closed system.

Black magnetite is precipitated when the iron source is added to the NaOH in the presence of N_2. Methods for aiding in the precipitation of magnetite include vigorous mechanical mixing for 30 min, addition of approximately 50 vol% of acetone, and use of an external magnet at the bottom of the reactor. The supernatant is removed and replaced by a mixture of 50 vol% deionized water and 50 vol% acetone. After decanting several times, the precipitate is divided into two portions. The first is dried in an oven at 120°C for 2 h and used as a powder for physical measurements. The other is redispersed in a proper aqueous solution as a ferrofluid and used for the absorption behaviors of microwave irradiation.

When the concentration of the NaOH solution is increased from 0.9 to 1.5 M at a pH = 14, the crystal size increases from 13 Å to 30 Å. On the other hand, the pH of the solution also plays an important role in controlling the crystal size. For solutions of 1.5 M NaOH, decreasing the pH from 14 to 11.5 has been shown to increase the particle size from 30 Å to 60 Å. The particle size distribution and morphology were examined by TEM analysis. A Langmuir film was prepared on a TEM grid in order to prepare a monodispersed magnetite layer. A

volume of 100 μL of magnetite in oleic acid was redispersed in 100 mL toluene with a strong sonification and the agglomeration was precipitated using a centrifuge. Then, 1 mL of ferrofluid was taken from the supernatant and redispersed in 100 mL toluene under strong sonification. The agglomeration was precipitated using a centrifuge and stabilized for 1 h before the 100 μL of the magnetite solution was removed from the top of the solvent and dropped into a deionized water bath, forming a thin Langmuir film on the surface of the water. The film was transferred onto a TEM grid using a horizontal dipping technique. As shown in Fig. 1, the SPIONs primarily consist of almost perfect mono particles, though their morphology ranges from ovular to spherical. The size distribution was calculated using an equation based on a log-normal function,[12] yielding an average particle diameter of 72 Å with a standard deviation $\sigma_d = 0.2$. This value is close to the crystal size calculated from XRD data (60 Å). The X-ray diffraction patterns show very low crystallinity at the interface, which induces a change in the magnetocrystalline anisotropy. The magnetic diameters, calculated from the Langevien equation, are also smaller than those determined by TEM. When the magnetite nanoparticles are crystalline, the interactions between the particles are larger than low crystalline particles. The magnetic size of the magnetic nanoparticles dispersed in a fluid and in powder form is reported in a previous paper.[13]

3.2. Electron Spin Resonance (ESR)

The microwave absorption by the sample is proportional to the imaginary component of the high frequency magnetic susceptibility. This susceptibility generally shows a resonance property with respect to the field due to Larmour precession of the magnetic moments around the DC magnetic field. The resonance field values and line width are determined by magnetic free energy and relaxation parameters, respectively. While the first integral of the field-derivative ESR signal represents the AC susceptibility, the second integral is proportional to the DC susceptibility. Therefore, ESR spectra present valuable information, including the DC and AC magnetic properties of the sample.

Fig. 2 shows the ESR spectra intensity of 1 nm SPIONs as a function of temperature, showing a behavior similar to typical spin-glass materials. Therefore, the magnetic moments of the individual 1 nm SPIONs are disordered throughout the sample, resulting in a sharp decrease in the magnetization as averaged over all possible random directions of the magnetic moments in single domain particles, due to spin frustration below 50 K. In particular, 11 nm SPIONs show a very broad maximum with respect to temperature. The magnetic anisotropy energy E_a is proportional either to the volume or to the surface of the particles in a single domain particle and becomes comparable with the thermal energy (k_BT).

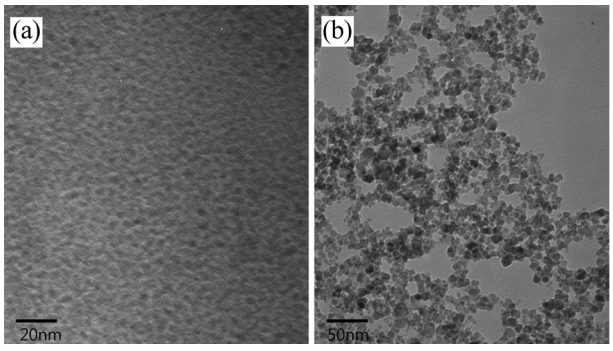

Fig. 1. TEM images of bare superparamagnetic iron oxide nanoparticles (SPIONs) prepared by coprecipitation method. The crystal sizes of (a) 1 nm and (b) 11 nm were measured by XRD.

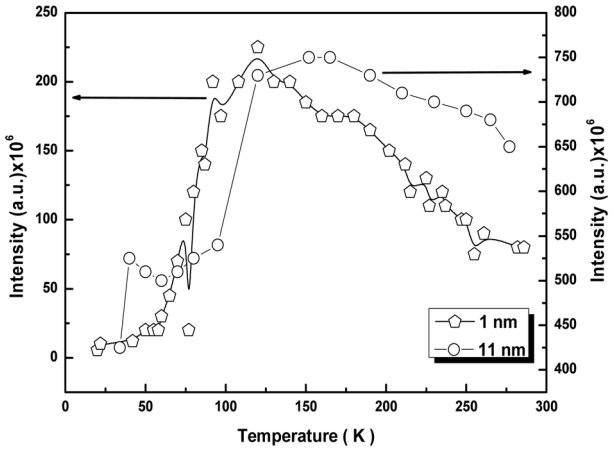

Fig. 2. ESR intensity versus temperature of 1 and 11 nm superparamagnetic iron oxide nanoparticles (SPIONs).

This effect is supported with the line width (ΔH_{pp}) data given in Fig. 3. At low temperatures, the ΔH_{pp} of 1 nm SPIONs rapidly increases and doubles with respect to that of 11 nm SPIONs. The decline of ΔH_{pp} at low temperature is related to the fact that the whole system can be considered magnetically solid, so relaxation times become longer, which is consistent to with the observed narrowing of ESR lines at low temperature. At low temperatures, ΔH_{pp} of the ESR spectra increases, showing linear temperature dependence. However, there is

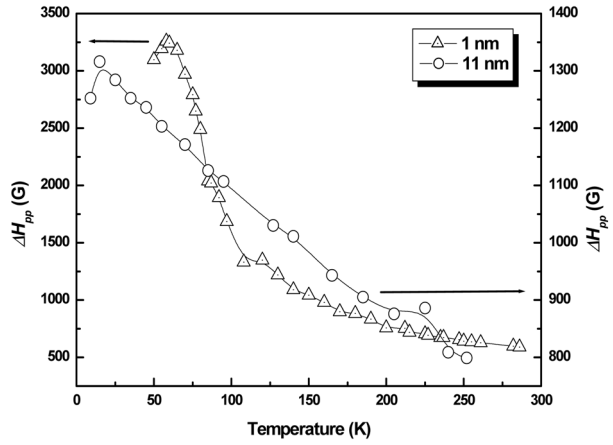

Fig. 3. ESR line-width versus temperature of 1 and 11 nm superparamagnetic iron oxide nanoparticles (SPIONs).

a deflection from linearity at very low temperatures. This ΔH_{pp} could be immediately ascribed to the dipolar interactions between the SPIONs. The decrease in the heterogeneity of the dipolar fields could be expected due to the ordering of the SPIONs. However, it was also expected that the linear temperature would be dependent on the magnetization parallel to the increments of magnetic moments of the individual particles, but the experimental results shown in Fig. 2 contradict this prediction. That is, at low temperatures, the disorder of the dipolar fields increases because the magnetization is not increasing at the same rate, which could be due to the effect of some antiferromagnetic interactions, thereby increasing the disorder of the system and enhancing the line broadening.

Effective g-values, which can be derived from the measurement of the magnetic field at the center of the ESR spectra, are given in Fig. 4. The temperature dependence of these values shows a linear behavior. The tendency of the g-value (the spectrum is shifted to the lower fields) shows an increase in the internal fields. This result is consistent with the line width results and both lines are superpositioned. The increment in effective g-values at low temperature should be attributed to the exchange anisotropy due to antiferromagnetic interactions between the SPIONs. Actually, the microscopic interactions of individual particles are antiferromagnetic, resulting in ferrimagnetic order. These antiferromagnetic microscopic interactions increase both the line width and the effective g-values. The main contributions to the ΔH_{pp} come from these interactions, as shown by Aktaş[14] in a study performed on a epitaxial single crystal Fe_3O_4 film on MgO substrate. Fig. 4 shows results consistent with Aktaş for 11 nm SPIONs, but the effect is more apparent. Therefore, the increase in the effective microscopic fields at low temperatures is obvious. In spin glass systems, this microscopic local field can usually be attributed to the exchange anisotropy.[14]

In conclusion, both samples show superparamagnetic behaviors. There are well-known dipole-dipole interactions between the magnetic nanoparticles. This dipolar interaction promotes either ferromagnetic or antiferromagnetic order, according to the position of the surrounding particles around a certain magnetic particle. Because of the magnetic interaction, the system is forced into a disorder, since the spin glass behavior cannot be attributed solely to the dipolar interactions. In particular, ΔH_{pp} for 1 nm SPIONs is too high (3 kG) to be explained by dipolar interactions between the particles. If this value is attributed to heterogeneous dipolar field distributions, this dipolar field must be at least 3 kG, contrary to the theoretical predictions. In these experiments, powders were diluted in paraffin in order to avoid dipole-dipole effects in the ΔH_{pp} parameter. However, sufficient homogeneity of the diluted sample could not be achieved due to magnetic dipole-dipole interactions between the particles.

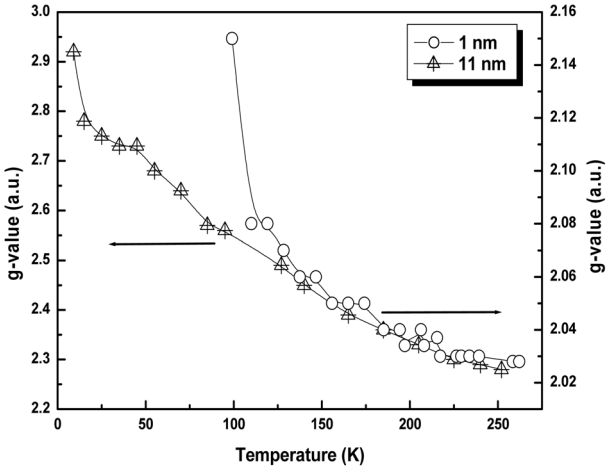

Fig. 4. g_{eff} values versus temperature of 1 and 11 nm superparamagnetic iron oxide nanoparticles (SPIONs).

On the other hand, the crystal structure of the ferrites changes from cubic to orthorhombic at low temperatures and the magnetization is slightly decreased. Moreover, the slight deviation from stoichiometry makes it difficult to achieve the maximum magnetization and widens the hysteric curve.

3.3. Microwave absorption by SPIONs

To analyze the temperature profiles for these experiments, conservation of energy was applied, considering the liquid sample to be homogeneous and isotropic. The conversion of microwave energy to thermal energy is governed by the relation[15]:

$$C_{\rho^{\rho}}\left(\frac{\partial T}{\partial t}\right)=\nabla(\kappa\nabla T)+\dot{Q} \tag{4}$$

where C_{ρ} is the heat capacity per unit volume, ρ is the mass density, T is the temperature (°C), t is the time(s), κ is the Boltzmann constant, and $\dot{Q}$ is the microwave energy absorption rate(J/s).

Holzwarth et al.[16] used a more simplified energy balance between the glass container and the sample in the microwave cavity. A Teflon container was chosen to avoid hybrid-heating effects, as a pre-experiment with a glass container showed that the glass was heated more than the sample. So, the energy equation was modified for a Teflon container:

$$\dot{Q}=m_S C_{ps}\frac{dT}{dt}+m_C C_{pc}\frac{dT}{dt}+kS(T-T_0) \tag{5}$$

where $\dot{Q}$ is the microwave energy absorption rate (J/s), S is the surface area of the container exposed to microwave irradiation (m^2), k is the heat-transfer coefficient ($J/m^{2o}C$ s), T is the temperature of the sample (°C), T_0 is the initial temperature of the system (°C), m is the mass (kg), C_p is the heat capacity (J/kg^oC), t is the time (s), and the subscripts s and c denote the liquid sample and the Teflon container, respectively.

Therefore, the solution of Eq. (5) is:

$$T=T_0+\frac{A}{B}(1-exp(-Bt)) \tag{6}$$

In Eq. (6), A (°C /s) and B (s^{-1}) denote the rates of energy absorption and heat loss for the microwave-irradiated system, respectively. Values of these parameters were obtained for

variously heated samples by non-linear fitting Eq. (6) to the experimental results.

Microwave absorption experiments were performed at 2.45 GHz with 800 W of irradiation output. A Teflon-shielded thermocouple was used to monitor the temperature change. Temperature fluctuations due to electromagnetic noise inside the sample were confirmed by a standard thermometer, after the main power was turned off. Abnormal temperature profiles were occasionally observed due to non-homogeneous microwave fields in the cavity. When this happened, the power was turned off and the experiment was repeated until the temperature profile was reproducible. Digital data was recorded every *ms* with a data acquisition system that allows the data to be best fit using Eq. 6. Data fitting was performed with a common fitted value for B (so that the heat-transfer coefficient was the same for all experiments), allowing A to take different values for each run. The microwave absorption rates for polar and nonpolar solvents are significantly different, since polar molecules easily couple with microwaves and rapidly produce heat, while nonpolar molecules cannot couple with microwaves. In general, the heat generation in the microwave field is caused by ionic polarization and dipole rotation of solvent molecules. Consequently, the polarity index (P) of the solvent is an important factor for the microwave absorption rate. The microwave absorption rate, A, for water (P = 10.2) and cyclohexane (P = 0.2) in a Teflon container were 1.55°C s^{-1} and 0.833°C s^{-1}, respectively. The microwave absorption rate of water is approximately twice as fast as cyclohexane. Fig. 5 presents the temperature profiles as a function of microwave irradiation time for water and magnetite colloids in toluene (P = 2.4) containing different concentrations of magnetite particles with a diameter of 11 nm. The unpaired electrons (Fe^{2+}, Fe^{3+}) are excited to a high energy state by the absorption of microwaves. The excited electron then changes its spin direction and relaxes into a ground state by emitting phonons. The coupling between the magnetic dipoles and microwave fields converts the radiation energy to heat.[17] The SPIONs coupled with the microwaves and increased the friction between the particle and molecule. When the concentration of the SPIONs is increased in the solvent, the friction between the particle and polar solvent also increased, resulting in the linear increase in the microwave absorption rates.

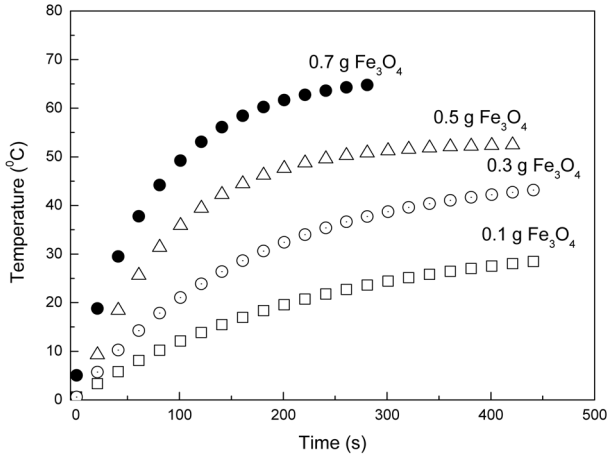

Fig. 5. Temperature profiles as a function of microwave (2.45 GHz) irradiation time for water and magnetite colloids in toluene containing different concentrations of magnetite particle (11 nm).

4. Conclusions

For application in hyperthermia, SPIONs with a diameter of 11 nm were prepared by controlled coprecipitation. Although a ferrimagnetic order makes it possible to get very high magnetization values, the exchange interactions are antiferromagnetic and the dipolar interactions are either ferromagnetic or antiferromagnetic, so it is not surprising to get a disordered spin profile known as spin-glass. The enormous increase in line width of the ESR spectra can be correlated to the distribution of exchange interaction. Indirect electron magnetic resonance experiments in the microwave cavity at 2.45 GHz with 800 W of irradiation output were performed. This approach allows for the prediction of heating mechanisms as a result of the excitation of unpaired electrons of iron, effects of coating agents, particle size, and volume fraction. The efficiency for converting microwave irradiation to thermal energy is predicted by applying the conservation of energy to a differential volume. The rates of heat loss and energy absorption are obtained by non-linear fitting of the experimental data.

Acknowledgment

This research was supported by the Basic Science Research Program through the National Research Foundation of Korea (NRF), funded by the Ministry of Education, Science and Technology (Grant No. 2011-0013675).

REFERENCES

1. Y. M. Wang, X. Cao, G. H. Liu, R. Y. Hong, Y. M. Chen, X. F. Chen, H. Z. Li, B. Xu, and D. G. Wei, "Synthesis of Fe_3O_4 Magnetic Fluid used for Magnetic Resonance Imaging and Hyperthermia," *J. Magn. Magn. Mater.,* **323** [23] 2953-59 (2011).
2. E. P. Hui, V. W. Y. Lui, C. S. C. Wong, B. B. Y. Ma, C. P. Y. Lau, C. S. F. Cheung, K. Ho, S. H. Cheng, M. H. L. Ng, and A. T. C. Chan, "Preclinical Evaluation of Sunitinib as Single Agent or in Combination with Chemotherapy in Nasopharyngeal Carcinoma," *Invest. New Drugs*, **29** [6] 1123-31 (2011).
3. D. Z. Chen, K. Engel, and C. Wang, "A New Algorithm for a Field Splitting Problem in Intensity-Modulated Radiation Therapy," *Algorithmica*, **61** [3] 656-73 (2011).
4. S. Yagyu, T. Iehara, T. Gotoh, M. Miyachi, Y. Katsumi, K. Kikuchi, K. Tsuchiya, S. Osone, H. Kuroda, T. Sugimoto, T. Sawada, and H. Hosoi, "Preoperative Analysis of 11q Loss Using Circulating Tumor-released DNA in Serum: A Novel Diagnostic Tool for Therapy Stratification of Neuroblastoma," *Cancer Lett.*, **309** [2] 185-89 (2011).

5. W. W. Tseng and S. P. L. Leong, "Long-term Survivors After Immunotherapy for Metastatic Melanoma," *Immunol. Lett.,* **139** [1-2] 117-18 (2011).
6. D. P. Santos, M. A. Ruiz, V. Gallardo, M. V. B. Zanoni, and J. L. Arias, "Multifunctional Antitumor Magnetite/chitosan-l-glutamic Acid (core/shell) Nanocomposites," *J. Nanopart. Res.,* **13** [9] 4311-23 (2011).
7. C. S. S. R. Kumar and F. Mohammad, "Magnetic nanomaterials for Hyperthermia-based Therapy and Controlled Drug Delivery," *Adv. Drug Deliv. Rev.,* **63** [9] 789-808 (2011).
8. S. Laurent, S. Dutz, U. O. Hafeli, and M. Mahmoudi, "Magnetic Fluid Hyperthermia: Focus on Superparamagnetic Iron Oxide Nanoparticles," *Adv. Colloid. Interface Sci.,* **166** [1-2] 8-23 (2011).
9. I. Pyykko, J. Zou, W. K. Zhang, and Y. Zhang, "Nanoparticle-based Delivery for the Treatment of Inner Ear Disorders," *Curr. Opin. Otolaryngol. Head Neck Surg.,* **19** [5] 388-96 (2011).
10. S. M. Zhou, Y. Q. Guo, J. Y. Zhao, L. F. He, C. L. Wang, and L. Shi, "Particle Size Effects on Charge and Spin Correlations in $Nd_{0.5}Ca_{0.5}MnO_3$ Nanoparticles," *J. Phys. Chem. C*, **115** [23] 11500-506 (2011).
11. L. Libioulle, A. Bietsch, H. Schmid, B. Michel, and E. Delamarche, "Contact-inking Stamps for Microcontact Printing of Alkanethiols on Gold," *Langmuir*, **15** [2] 300-4 (1999).
12. C. G. Granqvist and R. A. Buhrman, "Ultrafine Metal Particles," *J. Appl. Phys.,* **47** [5] 2200-219 (1976).
13. D. K. Kim, Y. Zhang, W. Voit, K. V. Rao, and M. Muhammed, "Synthesis and Characterization of Surfactant-coated Superparamagnetic Monodispersed Iron Oxide Nanoparticles," *J. Magn. Magn. Mater.,* **225** [1-2] 30-36 (2001).
14. S. B. Oseroff, S. W. Cheong, B. Aktas, M. F. Hundley, Z. Fisk, and L. W. Rupp, "Spin-Peierls State Versus Néel State in Doped $CuGeO_3$," *Phys. Rev. Lett.,* **74** [8] 1450-53 (1995).
15. J. Lasri, P. D. Ramesh, and L. Schachter, "Energy Conversion During Microwave Sintering of a Multiphase Ceramic Surrounded by a Susceptor," *J. Am. Ceram. Soc.,* **83** [6] 1465-68 (2000).
16. A. Holzwarth, J. F. Lou, T. A. Hatton, and P. E. Laibinis, "Enhanced Microwave Heating of Nonpolar Solvents by Dispersed Magnetic Nanoparticles," *Ind. Eng. Chem. Res.*, **37** [7] 2701-706 (1998).
17. C. Surig and K. A. Hempel, "Interaction Effects in Particulate Recording Media Studied by Ferromagnetic Resonance," *J. Appl. Phys.*, **80** [6] 3426-29 (1996).